Downloaded from rsta.royalsocietypublishing.org

PHILOSOPHICAL TRANSACTIONS OF THE ROYAL SOCIETY A MATHEMATICAL, PHYSICAL & ENGINEERING SCIENCES

The capillary effect promoting collision and agglomeration of inclusion particles at the inert gas –steel interface

The Royal Society

Phil. Trans. R. Soc. Lond. A 1998 **356**, 957-966
doi: 10.1098/rsta.1998.0200

Email alerting service Receive free email alerts when new articles cite this article - sign up in the box at the top right-hand corner of the article or click **here**

To subscribe to *Phil. Trans. R. Soc. Lond. A* go to: **http://rsta.royalsocietypublishing.org/subscriptions**

This journal is © 1998 The Royal Society

Downloaded from rsta.royalsocietypublishing.org

The Royal Society

The capillary effect promoting collision and agglomeration of inclusion particles at the inert gas–steel interface

By H. Shibata, H. Yin and T. Emi

Institute for Advanced Materials Processing, Tohoku University, Sendai 980-77, Japan

Gas bubbling and flux injection processes have been extensively used in metallurgical industries for several decades since the processes have been confirmed to be effective in removing impurity elements and non-metallic inclusions from liquid metals and improving the morphology of inclusions. Aiming at more effective use of gas and flux powder for injection refining to obtain higher quality products at lower cost, elucidation of the interfacial phenomena at inert gas–solid particle–liquid metal interfaces has become increasingly important. A new technique is presented to observe *in situ* the inclusions on steel melt, revealing collision/agglomeration characteristics of the inclusions.

Keywords: capillary interaction; inclusion; particle; steel melt; interface; agglomeration; laser microscope

1. Introduction

In our previous work, a confocal scanning laser microscope (CSLM) combined with an infrared image furnace (Chikama *et al.* 1996) was used as a new investigating tool, which has made it possible to carry out an *in situ* real-time observation of collision and agglomeration behaviour of inclusion particles on the surface of steel melts at high temperatures. On molten steel surfaces, a long-range strong attraction, which can extend to tens of micrometres, was clearly observed to operate between solid inclusion particles (Yin *et al.* 1997). The strong attraction results in a quick agglomeration of solid particles at the inert gas–steel melt interface, and hence enhances the growth and removal of solid inclusions as well as the reactions between flux particles and inclusions on bubble surface in injection metallurgy practice. It was also found that there was no such strong attraction between liquid inclusion particles on molten steel surfaces (Yin *et al.* 1997). The present work is intended to make clear the origin of the attraction force between inclusions partly immersed in the steel melt surface.

2. Experiment

A mirror-polished disc specimen (4.3 mm diameter × 2 mm) of steel was set into a high purity alumina crucible and placed in a 650 W image furnace chamber (described in detail in Chikama *et al.* (1996)). Before experiments, the furnace chamber, specimen and crucible were evacuated to 10^{-5} Torr for desorbing gases. Then, the specimen and crucible were baked at about 500 K for 1 h to remove absorbed moisture

© 1998 The Royal Society
TEX Paper

Downloaded from rsta.royalsocietypublishing.org

Table 1. *Compositions of steels studied and inclusion particles surfaced (mass%)*

grade name	concentration of elements in steel							composition of inclusions			
	C	Si	Mn	P	S	sol Al	total O	CaO	Al_2O_3	SiO_2	note
LCAK	0.038	0.01	0.20	0.010	0.010	0.035	0.0200	—	100	—	solid
Fe–3%Si	0.0006	3.35	0.01	0.001	0.001	0.001	0.0024	—	> 80	< 20	solid
HC–Ca	0.840	0.17	0.50	0.010	0.010	0.001	0.0030	< 20	> 80	—	solid
SK	0.001	0.45	0.13	0.002	0.003	0.001	0.0103	< 5	< 2	> 95	solid
HC–Ca	0.840	0.17	0.50	0.010	0.010	0.001	0.0030	~ 50	~ 50	—	liquid
SK	0.001	0.45	0.13	0.002	0.003	0.001	0.0103	~ 25	~ 50	~ 25	liquid
HSLA	0.048	0.31	1.17	0.006	0.0005	0.036	0.0015	> 30	~ 60	< 10	liquid

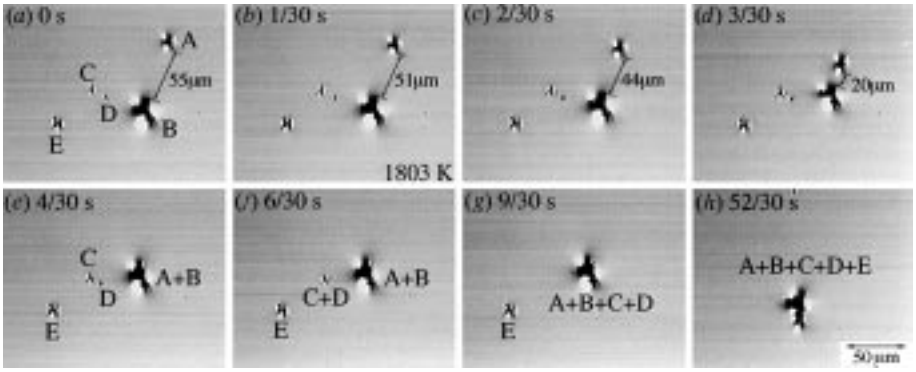

Figure 1. Sequence of long-range attraction, quick agglomeration and the cluster formation process of alumina inclusion particles observed on a LCAK steel melt surface at 1803 K with CSLM.

under the flow of highly purified Ar gas containing O_2, H_2O, CO_2 and CO gases of less than 10 ppb. After that, the specimen was heated to its melting point (usually *ca.* 1800 K) at 100 K min^{-1}. The experiment was carried out under the purified Ar atmosphere which was further deoxidized by pure titanium, heated to *ca.* 1700 K to prevent oxidation of the specimen surface. During the experiment, the dynamic pictures of the specimen surface, scanned by a He-Ne laser beam and monitored by CCD image sensor, were displayed on a CRT screen and recorded on a video-tape at $\frac{1}{30}$ s intervals (Yin *et al.* 1997). Interesting behaviour of inclusion particles is revealed and interparticle attraction forces deduced by analysing the recorded video image frame by frame. Composition of inclusion particles on the melt surface was determined by EPMA after quenching the molten specimen. The compositions of steel grades studied and the inclusions found on the specimen surfaces are listed in table 1.

3. Results

After the steel specimen was melted, many small inclusion particles surfaced from the steel bath. They quickly agglomerated and formed large clusters on the bath surface due to a long-range attraction operating between them. Various solid inclusion

Downloaded from rsta.royalsocietypublishing.org

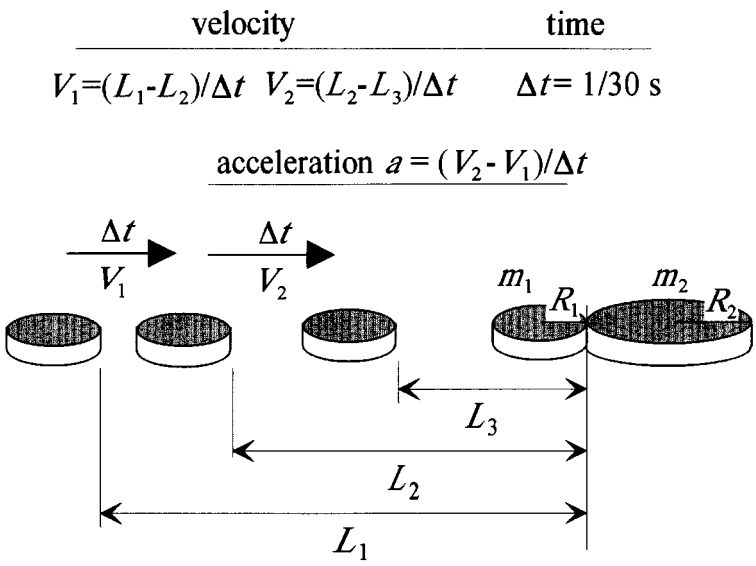

Figure 2. Schematic diagram to calculate acceleration from observed change in the position of disc-like inclusion particles.

particles, such as Al_2O_3, Al_2O_3–80 mass%SiO_2, CaO–80%Al_2O_3 and CaO–Al_2O_3–95%SiO_2, etc., observed on various steel melt surfaces, attracted each other strongly over a distance of a few tens of μm (described in detail in Yin *et al.* (1997)). An example of such an accelerated attraction between pure alumina particles A and B on LCAK molten steel surface is shown in figures 1*a–e*. The distance between the two particles is quickly decreased by the attraction from 55, 51, 44 to 20 μm at $\frac{1}{30}$ s intervals. The formation of clusters as induced by this attraction from A + B, C + D, (A + B) + (C + D) to A + B + C + D + E is shown in figures 1*e–h*.

To elucidate the nature of the long-range attraction, an approximate calculation of the magnitude of the attraction force is carried out using the observed acceleration with the estimated mass of the particles. The particle shape is approximated to be an elliptical disc, and the length of the long axis (d_1) and the short axis (d_2) of a particle is noted. Also, the height of all the discs is taken to be 2 μm on the basis of confocal observation of the thickness of alumina particles on the steel melt surface. Further, the elliptical disc is approximated to be circular, of radius R, which is taken to be equal to the geometric average, $R = \frac{1}{2}\sqrt{d_1 d_2}$. The acceleration, a_1, of the guest particle when the host particle in the particle pair stayed quiescent is determined from the change of the position of the guest particle at $\frac{1}{30}$ s intervals, as shown in figure 2. The attraction force, F, is then given by

$$F = m_1 a_1, \tag{3.1}$$

where m_1 is the mass of the guest particle. In this force analysis, the frictional force which arises from viscous drag of the particle by the liquid steel surface is ignored. Thus, the apparent attraction force operating between alumina solid particles is determined to be in the range of 10^{-16}–10^{-14} N, as shown in figure 3. Also, the acting length of the attraction, defined as L_1 in figure 2, is observed to be longer than 10 μm for particles with radius of larger than 2 μm. The force and its acting distance increase with the size of particle in a particle–particle pair, as shown in

Downloaded from rsta.royalsocietypublishing.org

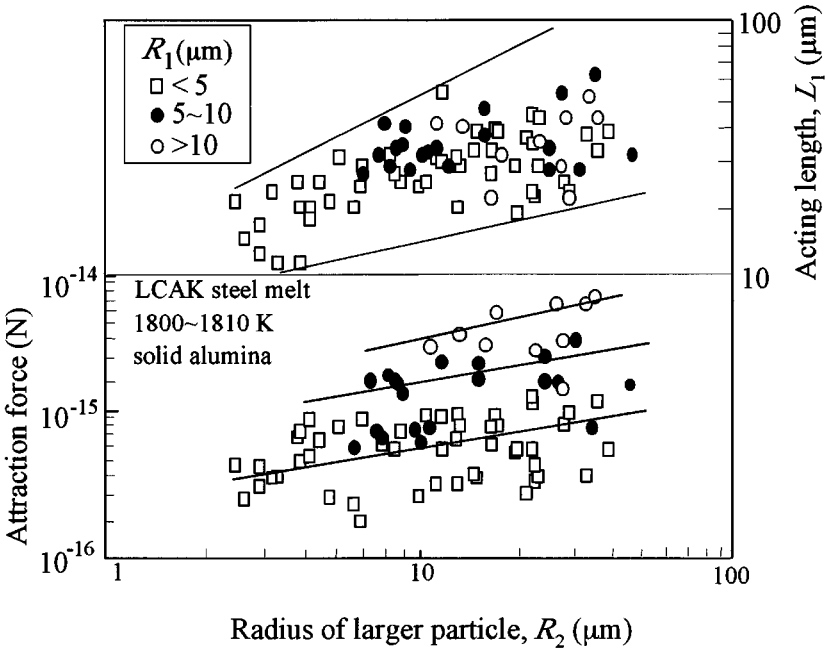

Figure 3. Observed long-range attraction force and its acting length versus size of alumina particle.

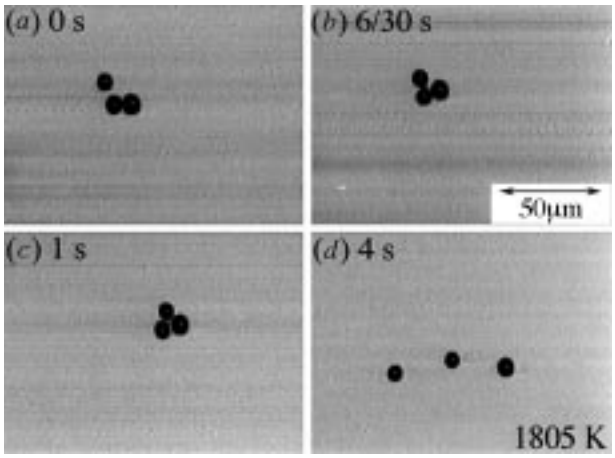

Figure 4. Touching and separation of liquid CaO–50%Al_2O_3 particles with random surface flow on an HC–Ca steel sample.

figure 3. In addition, the attraction force and acting length are not significantly influenced by surfactant elements, like sulphur, in molten steel (Yin *et al.* 1997).

On the other hand, no long-range attraction was observed on molten steel surfaces between all the kinds of liquid inclusion particles (Yin *et al.* 1997) listed in table 1. A typical case is shown in figure 4 where three 50%CaO–50%Al_2O_3 particles on the surface of HC–Ca steel melt come very close to each other as they are driven by a random surface flow. However, they move away subsequently without showing any attraction in between. According to our preliminary investigation (Yin *et al.* 1997), such long-range strong attraction cannot be attributed to the van der Waals force,

Downloaded from rsta.royalsocietypublishing.org

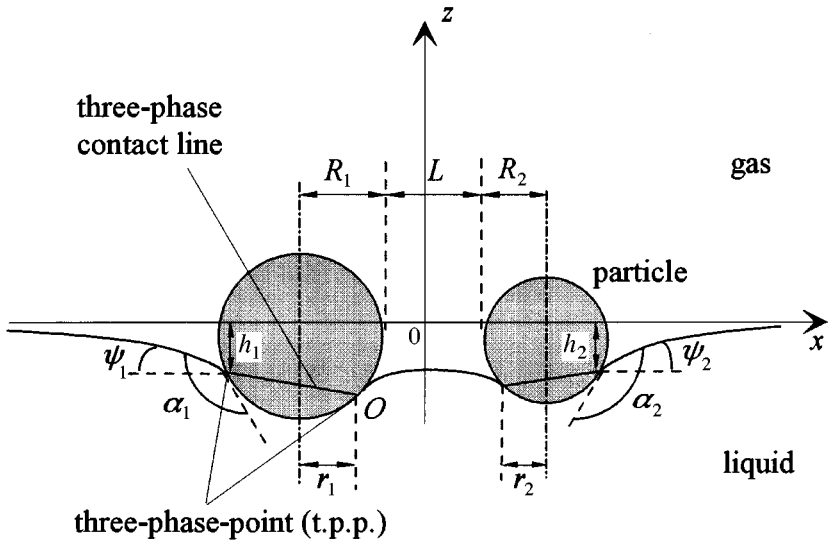

Figure 5. Schematic diagram of capillary meniscus around two spherical particles.

the Rayleigh–Benard flow of the steel melt (Pearson 1958), macroscopic local surface flow on the steel melt (Yin *et al.* 1997), the laser trapping effect (Ashkin 1970) or to coulombic interaction between solid inclusions on the steel melt surface.

4. Discussion

Capillarity causes a strong attraction between two floating solid bodies partly immersed in water when they come very close to each other. In terms of surface physics, the observed attraction between the solid inclusion particles partly immersed in molten steel may be the same as that in the gas–water system. An important parameter, capillary length, $q^{-1}(=[\Delta\rho g/\gamma]^{-1/2})$, was defined by Kralchevsky *et al.* (1994) to characterize the range of capillary interaction between solid particles at gas–liquid interfaces, and calculated to be 2.7 mm for the gas–water system. Here, $\Delta\rho = \rho_{\mathrm{L}} - \rho_{\mathrm{G}}$ (ρ_{L} and ρ_{G} are the density of liquid and gas phases), g is the acceleration due to gravity and γ is the surface tension of the liquid. According to this definition, the capillary length of an inert gas–molten steel system can be calculated to be 5.1 mm as the density and surface tension of molten steel are 7000 kg m^{-3} and 1.8 N m^{-1} (density of gas is negligible here). This comparison shows that the range of capillary interaction of a gas–steel melt system is longer than that of a gas–water system.

To confirm that the observed attraction is also caused by the capillary effect, the calculated order of magnitude of the capillary attraction must be the same as the observed order of magnitude. Paunov *et al.* (1993) theoretically derived an equation for the capillary interaction energy between two spherical particles 1 and 2 at a gas–liquid interface when their radius, R_i, is smaller then 100 μm as

$$\Delta W = -\pi\gamma \sum_{i=1}^{2} (Q_i h_i - Q_{i\infty} h_{i\infty})[1 + O(q^2 R_i^2)], \quad i = 1, 2, \tag{4.1}$$

where subscript i represents the particles 1 and 2, ∞ means that the separation between the two particles is infinite and $O(y)$ is the zeroth-order function of approximation. According to a series of equations derived by Paunov *et al.* (1993), Q_i

Downloaded from rsta.royalsocietypublishing.org

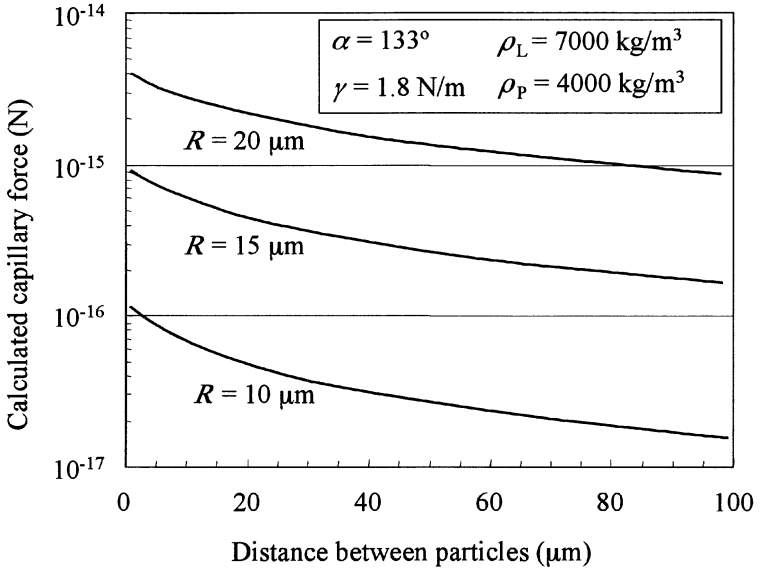

Figure 6. Dependence of calculated capillary force on the distance between two identical particles with varied size.

(defined as $r_i \sin\psi_i$; r is the radius of the three-phase contact line and ψ is the angle of meniscus slope) and the height difference (h_i shown in figure 5) at the separation, L, between the two particles can be calculated numerically.

Furthermore, when $L \to \infty$, $Q_{i\infty}$ was given by Chan *et al.* (1981) as

$$Q_{i\infty} = \tfrac{1}{6}q^2R_i^3(2 - 4D_i + 3\cos\alpha_i - \cos^3\alpha_i)[1 + O(qR_i)]. \tag{4.2}$$

Also, $h_{i\infty}$ is given by (Paunov *et al.* 1993)

$$h_{i\infty} = r_{i\infty}\sin\psi_{i\infty}\ln\frac{4}{\gamma_e q r_{i\infty}(1+\cos\psi_{i\infty})}, \quad (qr_{i\infty})^2 \ll 1, \tag{4.3}$$

where D is the density ratio of particle to liquid, α is the contact angle of particles and $\ln\gamma_e$ is the Euler–Masceroni constant.

Once ΔW is calculated at different L, the capillary interaction force is given by

$$F = \mathrm{d}(\Delta W)/\mathrm{d}L. \tag{4.4}$$

The value of F calculated from equations (4.1)–(4.4) with the data from a gas–alumina–molten steel system for a pair of two identical spherical particles of $R = 10$, 15 or 20 μm is shown in figure 6, where the capillary interaction between the particles is shown to be long range. This result agrees well with the present observation. For larger particles ($R > 20$ μm), the calculated force is of the same order of magnitude as that observed in figure 3, despite the difference in particle shape assumption between the observation and calculation. For smaller particles ($R < 10$ μm), however, the calculated force is one or two orders of magnitude smaller than the observed force in figure 3. If particle shape and viscous drag force are taken into account, the difference can be greater. Figure 7 compares observed with revised calculated data, where the particles are considered to be disc-like (Yin *et al.* 1998). Although the calculated data are two orders of magnitude smaller than the observed data, the fact that the slopes of the two lines are almost the same shows that the two forces share the same nature (Yin *et al.* 1998).

Downloaded from rsta.royalsocietypublishing.org

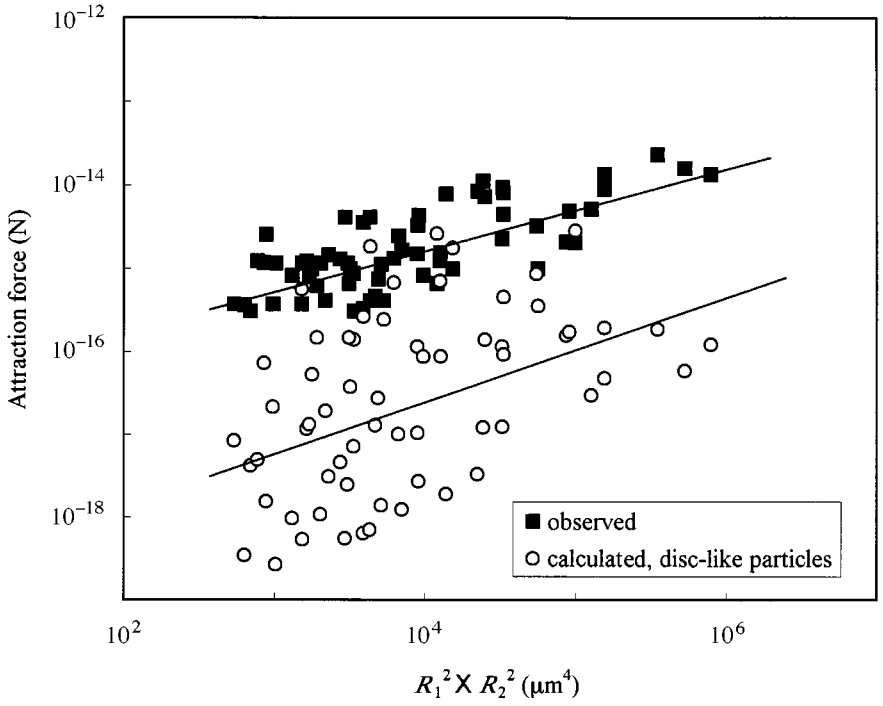

Figure 7. Comparison of calculated force with observed force versus $R_1^2 \times R_2^2$.

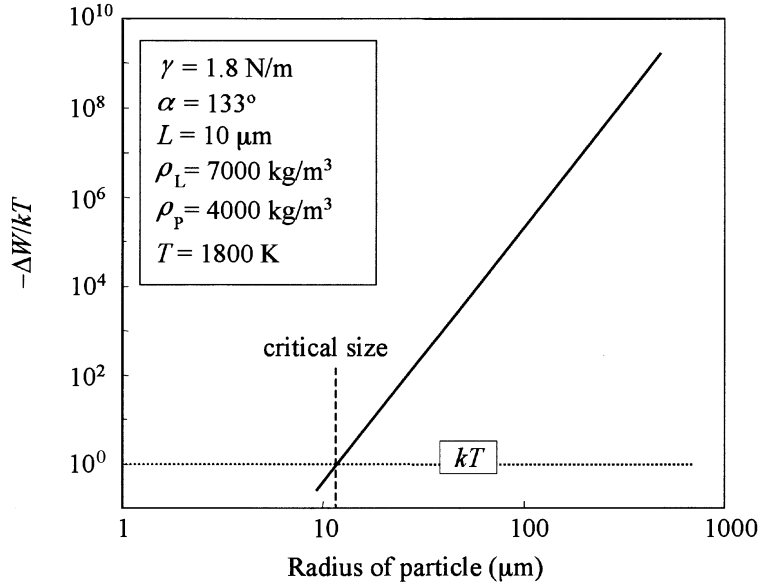

Figure 8. Chart of $-\Delta W/kT$ versus particle radius, R, for two identical particles at the gas–molten steel interface.

When the capillary interaction energy is compared with the thermal energy, kT (k is the Boltzmann constant and $T \approx 1800$ K), for a gas–alumina–molten steel system, the critical size of the particles, below which the capillary interaction is negligible,

Downloaded from rsta.royalsocietypublishing.org

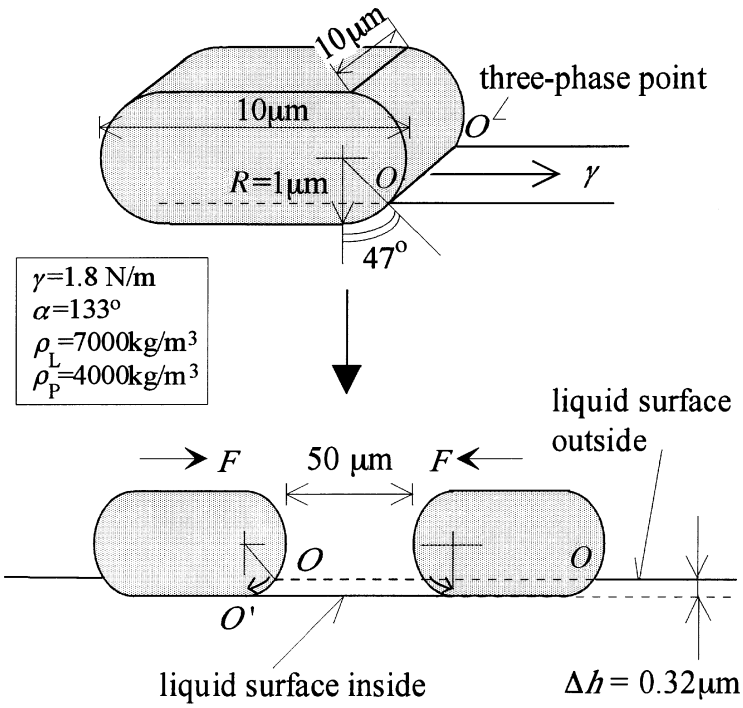

Figure 9. Schematic diagram of capillary attraction force calculation between particles on the melt surface by assuming that the liquid surface in between depresses down to the particle bottom.

can be estimated from figure 8. It is obvious here that, for particles with radii smaller than 15 μm, the capillary attraction is insignificant between alumina particles at the molten steel surfaces when the separation is greater than 10 μm. This conclusion is totally different from the present experimental observation. Actually, in most cases, alumina particles with radii of a few μm, like particles C and D in figure 1, are attracted to each other from about 10 μm away.

Some experimental data are available to support the above theoretical analysis for a system of two vertical cylinders of submillimetre diameter partly immersed in water (Velev 1993), which is fundamentally not that different from the two-sphere system. The theoretical calculation is in good agreement with the observation only at large separations (> 500 μm) between the two cylinders (Velev *et al.* 1993). For smaller separations, the observed capillary force is always stronger than the calculated capillary force because the linear superposition approximations made in the theoretical analysis cannot describe the capillary force well. The reason is that the superposition approximations are no longer linear when the separation gets small (Velev *et al.* 1993). However, no data have been reported to date to confirm the validity of the theory for the system of very small particles ($R < 20$ μm) at small separations of less than 50 μm.

Under these circumstances, a bold assumption is made for the system of small particles at small separations in the following force analysis. From the Laplace capillary equation (Bikerman 1970) and force balance analysis on particles (Schulze 1977) at steel melt surfaces, the height, h in figure 5, is calculated to be small (3.8 nm) for a spherical alumina particle with a radius of 10 μm. This result shows that the change

Downloaded from rsta.royalsocietypublishing.org

of melt surface profile can be totally ignored when a small alumina particle (of the order of a few μm) is located at a molten steel surface. Thus, a more precise example is depicted in figure 9, where a $10 \times 10 \times 2\ \mu m^3$ cuboid alumina particle with round edges is partly immersed in the steel melt surface.

When another cuboidal alumina particle comes close, at a distance of 50 μm, the steel melt surface in between will be dragged downward as the result of the capillary effect, leading to the depression of the three-phase point (TPP) O in figure 9. As the capillary depression is so large, a crude assumption is made here that the TPP will shift from O to the bottom, O', of particles in figure 9. The capillary force can then be calculated by (Bikerman 1970)

$$F = 0.5g(\rho_L - \rho_P)w\Delta h^2, \tag{4.5}$$

where, w is the width of the cuboid particle. After the same force balance analysis as mentioned above, the height is calculated to be 0.32 μm. In this case, the capillary attraction force, F, is calculated from equation (4.1) to be 1.5×10^{-14} N by ignoring the three-dimensional effect of the liquid surface. When the drag force of the melt surface acting on the particles during movement is subtracted, the capillary attraction becomes of the same order of magnitude as the observed attraction. The absence of long-range attraction between lens-like liquid particles at molten steel surfaces can be understood because the depression of the molten steel surface between the liquid particles cannot take place in view of their contact angles with molten steel, even when they come very close to each other.

Reservation should be made, however, that the shift of point O is dynamic when two particles come closer. Then, determining the precise position of the TPP in the dynamic process becomes complicated. Also, at the beginning of particle movement, the balance of capillary attraction and viscous drag force is difficult to analyse. Therefore, the estimation of the acting length of the capillary attraction remains an approximation.

5. Conclusions

In situ observed long-range attraction between solid particles on molten steel surfaces is mainly attributed to the capillary interaction when they get close to each other. This effect is useful in high-temperature metallurgy processes because it can accelerate the agglomeration of solid inclusion particles and reaction between solid inclusion particles and flux particles at the gas–molten metal interface.

References

Ashkin, A. 1970 *Phys. Rev. Lett.* **24**, 156.

Bikerman, J. J. 1970 *Physical surfaces*, ch. 1. New York: Academic.

Chan, D. Y. C., Henry, J. D. & White, L. R. 1981 *J. Colloid Interf. Sci.* **79**, 410.

Chikama, H., Shibata, H., Emi, T. & Suzuki, M. 1996 *Mat. Trans. JIM* **37**, 620.

Kralchevsky, P. A., Denkov, N. D., Paunov, V. N., Velov, O. D., Ivanov, I. B., Yoshimura, H. & Nagayama, K. 1994 *J. Phys. Condens. Matter* **6**, 395.

Paunov, V. N., Kralchevsky, P. A., Denkov, N. D. & Nagayama, K. 1993 *J. Colloid Interf. Sci.* **157**, 100.

Pearson, J. R. A. 1958 *J. Fluid Mech.* **4**, 489.

Schulze, H. J. 1977 *Int. J. Mineral Proces.* **4**, 241.

Downloaded from rsta.royalsocietypublishing.org

Velev, O. D., Denkov, N. D., Paunov, V. N., Kralchevsky, P. A. & Nagayama, K. 1993 *Langmuir ACS* **9**, 3702.

Yin, H., Shibata, H., Emi, T. & Suzuki, M. 1997 *ISIJ Int.* **37**, 936 and 946.

Yin, H., Emi, T., Shibata, H. & Kim, J. S. 1998 *2nd Int. Conf. on High Temperature Capillarity, Cracow, Poland, 29/6–2/7/1997.* (In the press.)

Discussion

J. C. Earnshaw (*Department of Pure and Applied Physics, University of Belfast, UK*). I have a comment and a question regarding Professor Emi's experiments.

(1) Capillary forces will, indeed, provide long-ranged attractive forces between solid objects on a liquid surface (Gifford & Scriven 1971; Chan *et al.* 1981). Their range, typified by the capillary length $\sqrt{\sigma/g(\rho_{\mathrm{s}}-\rho_{\mathrm{l}})}$ (where σ is the surface tension and $\rho_{\mathrm{s,l}}$ are the densities of the solid and liquid), can be of the order of 1 cm. While gravity plays an essential role in the conventional model (Gifford & Scriven 1971), Lucassen has recently shown that for irregular particles there is an extra contribution which is independent of gravity (Lucassen 1992). This force can become repulsive at very short distances. This may be significant in Professor Emi's experiment, as it could provide the freedom to restructure demonstrated by the aggregates in his video.

(2) Some of Professor Emi's graphs appear to show an attractive force which *increases* with increasing separation. If this is indeed the case, how are we to understand such an unusual behaviour?

T. Emi. (1) The capillary length (here ρ_{s} and ρ_{l} in the equation gievn in the comment should be replaced by ρ_{G} and ρ_{L}) in our case is calculated and given (§ 4) to be 5.1 mm. For the formation of aggregates and the subsequent aggregate clustering, the acting range of capillary forces is much longer than the repulsive forces after Lucassen, as evidenced in my video presentation at the Royal Society.

The repulsive force may play a role in the early stage of cluster densification when the aggregates are about to stick together at their tips under quiescent circumstances, where the capillary attraction may compare with the repulsive force, if any. In the later densification stage, however, sintering between the stuck aggregates in the cluster plays a more important role.

(2) I regret that the graphs presented were misleading. In reality, larger particles in a particle pair exhibit stronger attraction at increased distances. We were aware of this difficulty in the graphs, and rearranged them in our paper by taking the particle size as a parameter.

Additional references

Gifford, W. A. & Scriven, L. E. 1971 *Chem. Engng Sci.* **26**, 287.

Lucassen, J. 1992 *Colloids Surf.* **65**, 131.